Transcriptomic Analysis Reveals Multiple Pathways of Canine Parvovirus 2-Induced Programmed Cell Death in Host Cells

Haoyuan Ma, Kai Yu, Qiang Guo, Jialiang Xie, Siqi Zhang, and Xu Gao*

Laboratory for Animal Molecular Virology, Department of Veterinary Medicine, College of Agricultural, Yanbian University, Yanji 133002, China

Abstract. Canine parvovirus disease (CP) is a highly contagious viral illness in dogs caused by canine parvovirus 2 (CPV2), often leading to a poor prognosis for dog recovery. The lack of strong immunity against different subtypes of CPV2 leads to numerous cases of CP, and the specific mechanisms by which it causes the disease are not fully understood. Recent studies have shown that CPV2 can induce apoptosis in MDCK host cells, but the involvement of other programmed cell death processes induced by CPV2 remains unclear. This research utilized RNA-Seq to identify significant differences in gene expression, with the differentially expressed genes (DEGs) being enriched in various programmed cell death pathways. Moreover, CPV2 infection upregulated genes associated with cancer, suggesting potential viral carcinogenic risks. The goal of this study was to establish a theoretical framework for understanding the etiology of CPV2 and to assist in the development of targeted pharmaceutical interventions.

1 Introduction

Canine parvovirus disease (CP) is a severe infectious illness characterized by bleeding, caused by CPV2. CPV2 is a non-enveloped, single-stranded positive-sense DNA virus with a diameter of 25 nm[1]. It belongs to the Parvoviridae family and the Parvovirus genus. The predominant strain in China is currently CPV2, which has led to the emergence of other subtypes due to antigenic drift[2]. CPV2 causes a wide range of infections, affecting not only dogs but also specific mammalian hosts[3,4]. Dogs usually become infected by consuming vomit or feces from infected animals, and the infection occurs without any preexisting immunity or immunodeficiency. CPV2 presents with diverse clinical manifestations, such as myocarditis and enteritis[5]. Scholars have observed signs such as encephalitis, leukoencephalopathy, and cerebral abscesses in infected dogs and cats[6]. Vaccination is the primary method to prevent CPV2, which mutates rapidly, making it difficult to control[7].

The genomic size of CPV2 is approximately 5,000 base pairs (bp), containing two open reading frames (ORFs) and smaller or overlapping genes that are preferentially spliced from the same mRNA. This process produces two non-structural proteins (NS1 and NS2) and two structural proteins (VP1 and VP2)[8]. VP3 (predicted) is produced by the breakdown of approximately 20-25 amino acids from the N-terminus of the VP2 sequence and is found exclusively in complete viral capsid proteins[9,10]. The VP2 protein is the predominant capsid protein in CPV2, constituting 90% of the virus capsid[11]. It plays a crucial role in determining the host range and interactions between the virus and host[12]. The nonstructural proteins NS1 and NS2 are phosphorylated after synthesis, which regulates gene expression[13]. Upon entering the host, NS1 localizes to the nucleus and exhibits ATPase and helicase functions, which regulate the production of other proteins[14]. NS1 plays a crucial role in the viral replication process.

Following viral infection, cells undergo programmed cell death (PCD) to manage damage responses and internal repair, maintaining homeostasis and essential functions[15,16]. This process aims to prevent the generation and release of progeny viruses. Common modes of PCD include apoptosis, necroptosis, pyroptosis, autophagy, ferroptosis, among others[17,18]. Studies have shown that many viruses in the Parvoviridae family, such as rat parvovirus H-1, induce apoptosis in host cells and can trigger cell death by arresting the cell cycle at the G2 phase in mouse host cells[19]. This activation initiates various death pathways in different cell types, with a significant impact observed in tumor cells. For example, Yan et al. demonstrated that goose parvovirus (GPV) infection reduces mitochondrial membrane potential, generates reactive oxygen species (ROS), and activates apoptosis-inducing factor (AIF) in host cells[20]. Similarly, Lin et al. found that mink enteritis virus (MEV) can induce apoptosis in F81 non-host cells[21]. However, there is limited research on PCD involving CPV2. To further investigate the pathogenic mechanism of CPV2 on the host, this study infected MDCK cells with the CPV2 strain obtained by our research group in previous work. This investigation aims to establish a

* Corresponding author: gaoxu@ybu.edu.cn

foundation for understanding the infection process of CPV2.

2 Materials and methods

2.1 Cell culture and viral infection

MDCK cells were stored in our research group's laboratory using culture media consisting of 90% DMEM (BOSTER, USA), 10% FBS (Gibco, USA), and 1% antibiotics. The cells were incubated at 37°C with 5% CO2 until reaching 80% adhesion density in T25 flasks. Subsequently, the cells were infected with CPV2 at MOIs of 0.02, 0.2, and 2, while the control group remained virus-free. Both the infected and mock groups were cultured for 24 hours in a cell incubator, and the CCK-8 activity was assessed in all four groups of cells.

2.2 RNA sequencing and transcriptomic analysis

MDCK cells were infected with CPV2 at an MOI of 1, and 24 hours later, cell RNA was extracted using TRIzol (TaKaRa, Japan). The integrity, concentration, and purity of the RNA were evaluated through RNA-specific agarose gel electrophoresis. The mRNA was fragmented into 200-300 bp fragments by ion disruption and used as a template for cDNA synthesis with reverse transcriptase. The cDNA was then amplified via PCR to create a gene library, which was quality-checked. Subsequent sequencing was performed on the Illumina platform. Further details of the experimental procedures can be found in the supplementary data.

2.3 Flow cytometry analysis

A DNA staining solution was prepared by combining Triton X-100, propidium iodide (PI), RNase, and 1× PBS. After a 24-hour incubation period, the cells were harvested in a flow tube, washed, treated with pre-cooled 75% ethanol, and fixed overnight at -20 °C. Subsequently, PBS was added, and after centrifugation, the cells were stained with the DNA staining solution. Following a 30 min incubation at room temperature in the dark, flow cytometry was used to determine the lowest loading rate. In a separate procedure, cells collected after 24 h were washed and treated with Fluo-3 AM staining solution to create a single-cell suspension. The suspension was incubated at 37°C for 30 minutes in the dark to detect Ca^{2+} levels using flow cytometry.

2.4 Western blotting

Cellular proteins were extracted using RIPA lysis buffer supplemented with PMSF (Solarbio, Beijing). The protein concentration was then determined using a BCA assay (TaKaRa, Japan). Western blot experiments were conducted to analyze protein expression levels. Immunoblotting was performed with the appropriate primary antibodies, including anti-p53 (Proteintech, Wuhan), anti-p-MAPK (Proteintech, Wuhan), anti-p-JNK (Proteintech, Wuhan), anti-p-ERK (Proteintech, Wuhan), anti-HIF-1 (Proteintech, Wuhan), and anti-GAPDH (AB0036, Abways, Shanghai) antibodies.

2.5 Statistical analysis

The statistical software GraphPad Prism 8.0.2 was utilized to perform one-way analysis of variance (ANOVA) on the experimental results. Various multiple comparison methods, including normal and lognormal tests, were employed to assess the significance of the data. In this analysis, significance levels were denoted as follows: ***P<0.001 and **P<0.01 for extremely significant differences, and *P<0.05 for significant differences.

3 Results and discussion

3.1 RNA-Seq of CPV2-infected MDCK cells

Following RNA extraction using the TRIzol method and subsequent verification of RNA purity and concentration with a Nanodrop, transcriptome sequencing was conducted. Utilizing the R package ggplot2 for transcriptome sequencing analysis, we generated volcano plots illustrating differentially expressed genes (DEGs). Our findings revealed that approximately 2038 genes were upregulated, while 1396 genes were downregulated in the infected group compared to the control group, resulting in a total of 3434 DEGs (Figure 1a). The filtered reads were aligned to the reference genome using the updated version of TopHat2, known as HISAT2 (http://ccb.jhu.edu/software/hisat2/index.shtml).
HISAT2 utilizes an enhanced Burrows–Wheeler transform (BWT) algorithm, leading to improved speed and reduced resource consumption. Default parameters were applied for non-strand-specific libraries during HISAT2 alignment, whereas for strand-specific libraries, the library type needed to be specified.

A strong correlation was observed between apoptosis and autophagy genes during protein–protein interactions (PPI) network analysis of genes with significant patterns. A PPI study indicated that *ATG5* and *ATG7*, likely through protein interactions, maintain a balance between apoptosis and autophagy triggered in MDCK cells post-CPV2 infection (Figure 1b). Further examination of the apoptosis pathway highlighted substantial interactions involving cytochrome C (*Cyt C*), caspase9, and caspase7, with distinct expression patterns in the transcriptome data, suggesting their potential importance as key genes in the mitochondrial apoptosis pathway. Exploration of autophagy pathway-related genes uncovered a noteworthy association with unc-51-like autophagy activating kinase 1 (*ULK1*/*ATG1*), implying a potentially crucial role for *ULK1* in CPV2-induced autophagy in MDCK cells.

Kyoto Encyclopedia of Genes and Genomes (KEGG) pathway enrichment analysis identified significant pathways, including DNA replication, ribosome biogenesis in eukaryotes, RNA polymerase, and the cell

cycle. Following CPV2 infection in MDCK cells, multiple genes were found to be enriched in pathways linked to cancer, such as cellular senescence, the Forkhead Box O (*FoxO*) signaling pathway, and microRNAs in cancer (Figure 1c). Gene Ontology (GO) enrichment analysis indicated that the differentially expressed genes (DEGs) were predominantly associated with membrane-enclosed structures, organelle lumens, the nucleus, and intracellular organelle lumens, with the nucleus showing the highest level of enrichment (Figure 1d).

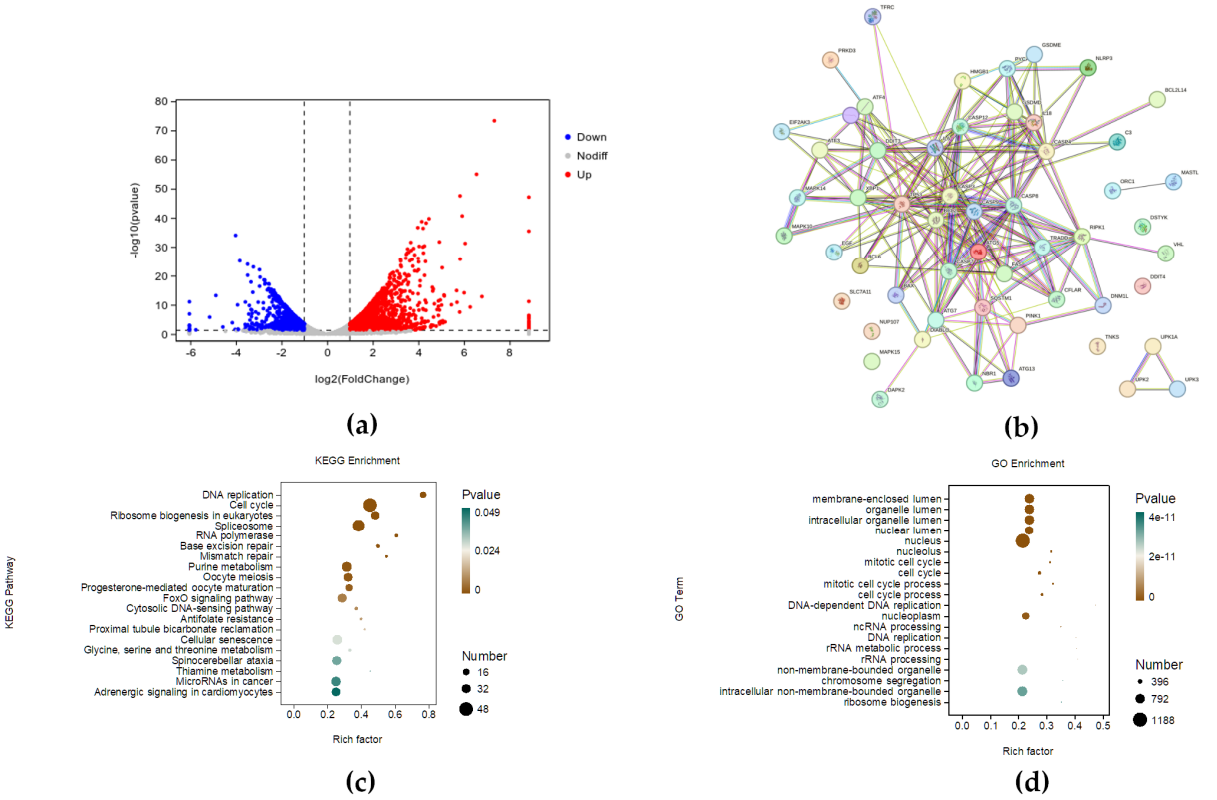

Figure 1. Transcriptome sequencing of MDCK cells infected with CPV2. (a). Volcanic map of eukaryotic reference transcriptome analysis. (b). The PPI network of apoptosis- and autophagy-related proteins in MDCK cells infected with CPV2. (c). KEGG enrichment analysis of the transcriptome. (d). GO enrichment analysis of the transcriptome. E. Gene expression enrichment in different pathways in the transcriptome.

3.2 Infection with CPV2 triggers the activation of cancer-related pathways in MDCK cells

Subsequent analysis of transcriptome data revealed significant alterations in gene expression. Uroplakins 3A (*UPK3A*), *UPK1A*, and *UPK1B*, proteins associated with the urothelial epithelium, were found to be significantly upregulated, while *UPK2* was downregulated. *UPK2* is crucial for the diagnosis of urothelial carcinoma (UC) and is typically expressed consistently in healthy cells, playing a role in cellular defense mechanisms. However, its expression may deviate under specific stimuli or in malignant cells. The increased expression of *UPK1A* and *UPK3A* genes suggests cellular translocation, particularly implicating these genes in the progression of urothelial cancer. Based on these findings, we propose a hypothesis that CPV2 may have the potential to induce viral carcinogenesis. Equations should be centred and should be numbered with the number on the right-hand side.

Through enrichment analysis of differentially expressed genes in the KEGG pathway, we observed a significant alteration in the bladder cancer pathway, with a notable increase in *UPK3A* expression suggesting potential carcinogenesis in the host cell line MDCK. Our findings also indicated a strong correlation between elevated *UPK3A* expression and reduced levels of tumor suppressor gene *p53* and death-associated protein kinase (*DAPK*). The activation of *DAPK* is intricately linked to endoplasmic reticulum stress and DNA promoter methylation, primarily driven by endoplasmic reticulum stress. This activation subsequently leads to the downregulation of cell cycle proteins specific to the G1/S phase via the *MAPK* signaling pathway, potentially inducing cell cycle arrest at the S phase. Furthermore, UPK3A activation triggers an increase in vascular endothelial growth factor (*VEGF*), often associated with the activation of hypoxia pathway genes (*HIF-1*, hypoxia-inducible factor 1) and calcium blockade. Overall, following CPV2 infection of MDCK cells, cellular damage and carcinogenesis appear to occur, with implications beyond programmed cell death pathways.

Building upon previous research, our study further investigated the potential pathway proteins associated with bladder cancer. Our findings revealed a significant decrease in *p53* levels, accompanied by a strong expression of *HIF-1*. Additionally, we observed notable

variations in the expression of *MAPK* family proteins, suggesting changes in cellular mitosis and proliferation (Figure 2b). Subsequently, we validated the cell cycle and Ca^{2+} levels by enriching the aforementioned pathways. Alterations in the cell cycle could impact the onset and advancement of apoptosis by hastening the process and increasing the chances of DNA replication errors and damage, ultimately leading to apoptosis. The processes of assessing the cell cycle post-infection and confirming the presence of apoptosis are tightly connected. Flow cytometry was employed to examine the cell cycle following inoculation with CPV2. The percentages of cells in the synthesis phase (S phase) were 59.14%, 40.78%, and 39.04% for the 2 MOI, 0.2 MOI, and 0.02 MOI infection groups, respectively, which were notably higher than the 35.67% in the control group. In the control group, the percentage of cells in the presynthesis phase (G1 phase) was around 61.22%. This percentage was higher than that in the experimental groups, where the percentages were 59.19% for an MOI of 2, 57.5% for an MOI of 0.2, and 40.1% for an MOI of 0.02. The distribution of cells in the G2/M phase closely resembled that in the G1 phase. Based on these results, infection of MDCK cells with CPV2 leads to arrest in the S phase, aligning with the transcriptome data (Figure 2c-d).

Excessive accumulation of Ca^{2+} in cells can induce apoptosis, as Ca^{2+} serves as a crucial signaling molecule within the cell. Ca^{2+} is involved in various apoptotic signaling pathways, such as the tumor necrosis factor pathway, mitochondrial pathway, ER stress pathway, and DNA damage pathway. Intracellular Ca^{2+} concentration can be used as an indicator of apoptosis. Flow cytometry analysis using Fluo-3 AM staining solution was conducted to assess the Ca2+ levels in MDCK cells infected with CPV2. The data revealed that in the 2 MOI, 0.2 MOI, and 0.02 MOI infection groups, the relative calcium ion contents were 66.17%, 48.63%, and 43.98%, respectively. These values were significantly higher at 41.62% with increasing multiplicity of infections compared to the control group (Figure 2e-f).

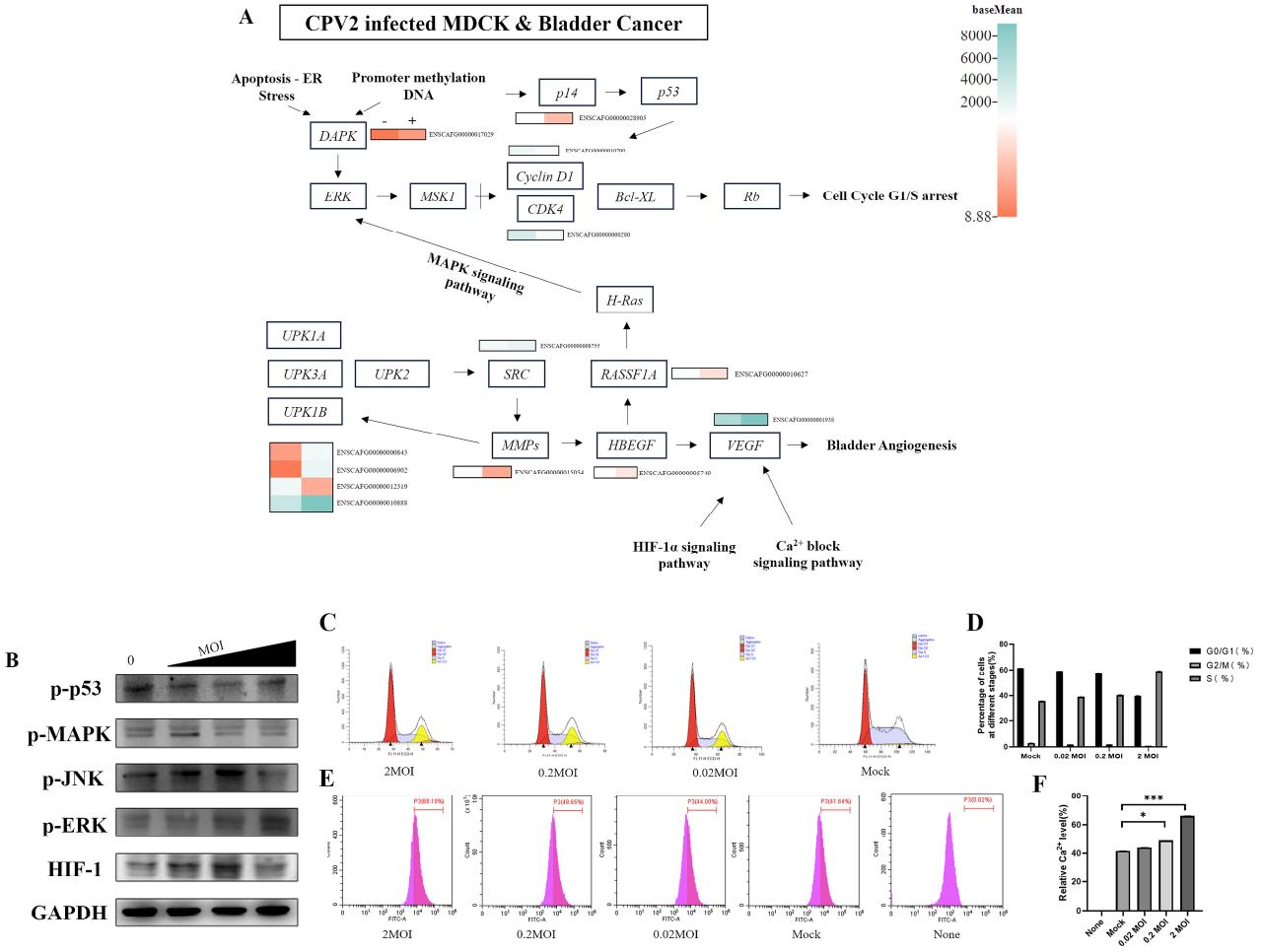

Figure 2. Infection with CPV2 leads to considerable activation of markers associated with the bladder cancer pathway in MDCK cells. (a). Transcriptomic sequencing revealed genes that are expressed in the bladder cancer pathway following CPV2 infection. (b). Western blot analysis was conducted to assess the expression levels of proteins associated with specific pathways in bladder cancer. (c). Flow cytometry analysis of the cell cycle status post-CPV2 infection. (d). The rate of cell cycle arrest at different phases under different CPV2 viral titers. (e). The expression levels of Ca^{2+} were measured after CPV2 infection of MDCK cells at MOIs of 2, 0.2, and 0.02. Additionally, a mock group and an untreated group without the Fluo-3 AM probe were included. (f). Effects of Ca^{2+} on different MDCK cells.

3.3 CPV2 infection activated multiple programmed cell death (PCD) pathways in MDCK cells

The elucidation of the cell death mechanism through a single pathway is not feasible due to its intricate nature. Therefore, a pathway enrichment map was created for MDCK cells infected with CPV2, focusing on variables with significant expression changes post-infection (Figure 3). The results suggest that upon infection with CPV2, there is a marked enrichment of genes involved in pathways related to apoptosis, autophagy, necrosis, and pyroptosis, indicating that various modes of cell death occur through coordinated interactions across multiple pathways. Noteworthy changes in the apoptotic process involve the genes *PARP* and *Cyt C*. In the control group, *Cyt C* expression was approximately 3.6 times higher than in the infected group, while PARP expression in the control group was about 2.2 times higher than in the infected group. Upon viral stimulation, PARP expression increases significantly in the early stages of infection to repair DNA damage or replication delays caused by the virus. However, in the later stages of infection, PARP activity is inhibited due to the accumulation of damaged DNA, leading to genomic instability in PARP and triggering cell apoptosis. In the absence or dysfunction of *Cyt C*, the electron transport chain in oxidative phosphorylation is disrupted, impeding ATP production, and ultimately causing cell death. Among the differentially expressed genes, the direct IAP-binding mitochondrial protein (*DIABLO*) plays a critical role as a signaling molecule that enhances the expression of apoptosis-related proteins within mitochondria. In its unbound state, *DIABLO* interacts with the X-linked inhibitor of apoptosis protein (*XIAP*) to prevent the inhibition of caspase synthesis, particularly caspases 3, 7, and 9. Our analysis revealed a significant upregulation of caspase7 and caspase12 in the transcriptome data, with levels in the infected group being approximately 2-3 times higher than those in the control group. Caspase7 and caspase12 are key genes involved in cell death pathways, which are typically activated during endoplasmic reticulum (ER) stress. In addition to caspase family proteins, apoptosis-inducing factors (*AIFs*) have been identified in the mitochondrial inner membrane. *AIF* is distinct from caspase-induced apoptosis and exhibited a 2-fold increase in the infected group compared to the control group. These results indicate that CPV2 infection in MDCK cells primarily induces apoptosis through the mitochondrial and endoplasmic reticulum pathways, while also activating caspase-independent cell apoptosis pathways.

The genes encoding tumor necrosis factor (*TNF*) and *TNFRSF1A*, which are associated with the death domain (*TRADD*) and are part of the exogenous pathway, exhibited distinct changes in expression following infection. Beyond *TNF* and *TRADD*, cells can also activate the death receptors Fas and Fas Ligand (*Fas L*) post-infection. This activation further initiates the execution factor caspase8 of the exogenous apoptosis pathway. Caspase8 plays a critical role in programmed cell death by both activating the terminal execution factor caspase3 and interacting with the important gene receptor-interacting protein kinase 1 (*RIPK1*), which is implicated in cell necrosis. *RIPK1* also stimulates the cellular necrosis pathway. Alongside caspase8, the activation of sequestosome 1 (*SQSTM1/p62*) can also lead to cell necrosis. The *p62* gene is essential for cellular autophagy, contributing to autophagy through various mechanisms. It is often used in conjunction with the microtubule-associated protein 1 light chain 3 (*LC3*) protein to assess the regularity of autophagic flux.

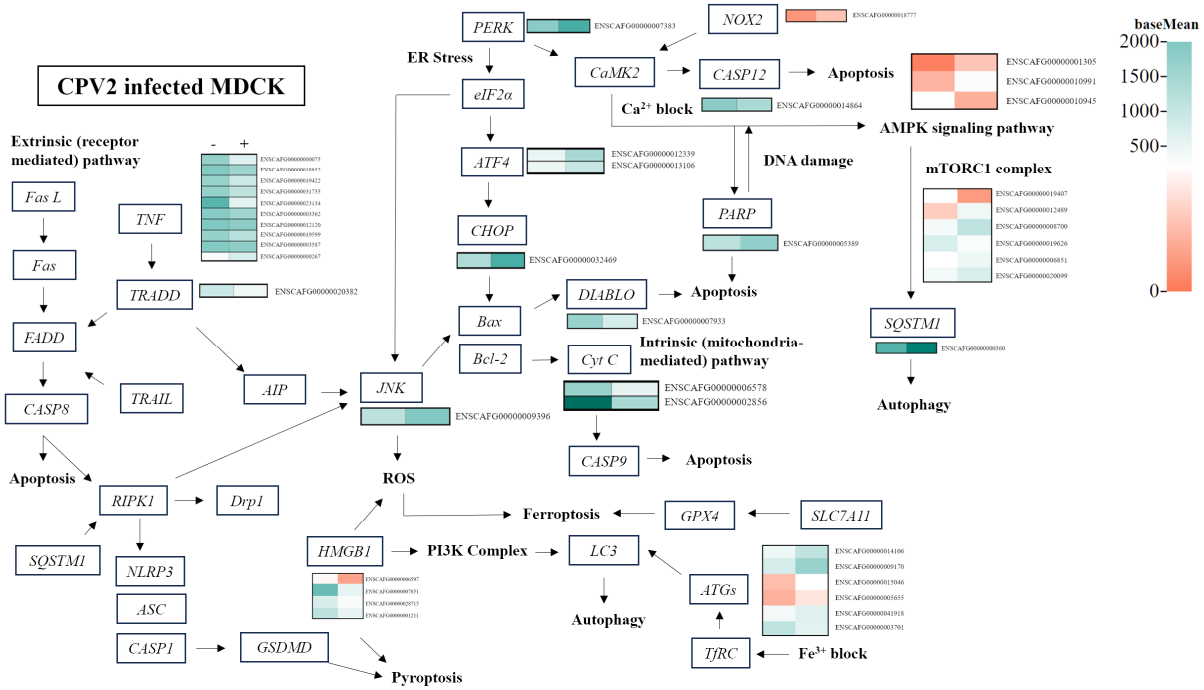

Figure 3. The pathway was enriched with divergent genes following CPV2 infection in MDCK cells.

KEGG pathway enrichment analysis indicated that genes in the *ATG* family not only initiate autophagy but also influence the mechanisms of ferroptosis. This suggests that an excess of intracellular iron can activate genes in the ATG family, thereby enhancing cellular autophagy. Furthermore, the high mobility group box-1 protein (*HMGB1*) can induce autophagy through the *PI3K* complex, but it may also trigger cell necrosis, possibly via a mechanism different from that of gasdermin D (*GSDMD*). As a result, given the changes in gene expression in MDCK cells following CPV2 infection, we next investigated different pathways of programmed cell death.

4 Conclusion

In conclusion, the present study demonstrates that infection with CPV2 induces significant programmed cell death in MDCK host cells. This pathological process is accompanied by marked alterations in the expression profiles of genes associated with cancer and cell cycle regulation. These findings elucidate the molecular mechanisms underlying CPV2 pathogenesis and provide a critical theoretical foundation for the future development of targeted therapeutic drugs against CPV2.

References

1. Appel, M. J.; Cooper, B. J.; Greisen, H.; Scott, F.; Carmichael, L. E., Canine viral enteritis. I. Status report on corona- and parvo-like viral enteritides. Cornell Vet **69** (3), 123-133 (1979).
2. Pan, S.; Jiao, R.; Xu, X.; Ji, J.; Guo, G.; Yao, L.; Kan, Y.; Xie, Q.; Bi, Y., Molecular characterization and genetic diversity of parvoviruses prevalent in cats in Central and Eastern China from 2018 to 2022. Front Vet Sci **10**, 1218810 (2023).
3. Parrish, C. R., Pathogenesis of feline panleukopenia virus and canine parvovirus. Baillieres Clin Haematol **8** (1), 57-71 (1995).
4. Parrish, C. R., Host range relationships and the evolution of canine parvovirus. Vet Microbiol **69** (1-2), 29-40 (1999).
5. Tuteja, D.; Banu, K.; Mondal, B., Canine parvovirology - A brief updated review on structural biology, occurrence, pathogenesis, clinical diagnosis, treatment and prevention. Comp Immunol Microbiol Infect Dis **82**, 101765 (2022).
6. Decaro, N.; Desario, C.; Amorisco, F.; Losurdo, M.; Colaianni, M. L.; Greco, M. F.; Buonavoglia, C., Canine parvovirus type 2c infection in a kitten associated with intracranial abscess and convulsions. J Feline Med Surg **13** (4), 231-236 (2011).
7. Decaro, N.; Buonavoglia, C.; Barrs, V. R., Canine parvovirus vaccination and immunisation failures: Are we far from disease eradication? Vet Microbiol **247**, 108760 (2020).
8. Qi, S.; Zhao, J.; Guo, D.; Sun, D., A Mini-Review on the Epidemiology of Canine Parvovirus in China. Front Vet Sci **7**, 5 (2020).
9. Singh, P.; Kaur, G.; Chandra, M.; Dwivedi, P. N., Prevalence and molecular characterization of canine parvovirus. Vet World **14** (3), 603-606 (2021).
10. Tsao, J.; Chapman, M. S.; Agbandje, M.; Keller, W.; Smith, K.; Wu, H.; Luo, M.; Smith, T. J.; Rossmann, M. G.; Compans, R. W.; et al., The three-dimensional structure of canine parvovirus and its functional implications. Science **251** (5000), 1456-1464 (1991).
11. Weichert, W. S.; Parker, J. S.; Wahid, A. T.; Chang, S. F.; Meier, E.; Parrish, C. R., Assaying for structural variation in the parvovirus capsid and its role in infection. Virology **250** (1), 106-117 (1998).
12. Miranda, C.; Thompson, G., Canine parvovirus: the worldwide occurrence of antigenic variants. J Gen Virol **97** (9), 2043-2057 (2016).
13. Kwak, S. H.; Kim, H.; Yun, H.; Lim, J.; Kang, D. H.; Kim, D., Characterization of Natural Compounds as Inhibitors of NS1 Endonuclease from Canine Parvovirus Type 2. J Microbiol Biotechnol **33** (6), 788-796 (2023).
14. Niskanen, E. A.; Ihalainen, T. O.; Kalliolinna, O.; Häkkinen, M. M.; Vihinen-Ranta, M., Effect of ATP binding and hydrolysis on dynamics of canine parvovirus NS1. J Virol **84** (10), 5391-5403 (2010).
15. Liu, J.; Hong, M.; Li, Y.; Chen, D.; Wu, Y.; Hu, Y., Programmed Cell Death Tunes Tumor Immunity. Front Immunol **13**, 847345 (2022).
16. Kopeina, G. S.; Zhivotovsky, B., Programmed cell death: Past, present and future. Biochem Biophys Res Commun **633**, 55-58 (2022).
17. Elmore, S., Apoptosis: a review of programmed cell death. Toxicol Pathol **35** (4), 495-516 (2007).
18. Park, W.; Wei, S.; Kim, B. S.; Kim, B.; Bae, S. J.; Chae, Y. C.; Ryu, D.; Ha, K. T., Diversity and complexity of cell death: a historical review. Exp Mol Med **55** (8), 1573-1594 (2023).
19. Hristov, G.; Krämer, M.; Li, J.; El-Andaloussi, N.; Mora, R.; Daeffler, L.; Zentgraf, H.; Rommelaere, J.; Marchini, A., Through its nonstructural protein NS1, parvovirus H-1 induces apoptosis via accumulation of reactive oxygen species. J Virol **84** (12), 5909-5922 (2010).
20. Yan, Y. Q.; Jin, L. B.; Wang, Y.; Lu, S. Y.; Pei, Y. F.; Zhu, D. W.; Pang, F. S.; Dong, H.; Hu, G. X., Goose parvovirus and the protein NS1 induce apoptosis through the AIF-mitochondrial pathway in goose embryo fibroblasts. Res Vet Sci **137**, 68-76 (2021).
21. Lin, P.; Cheng, Y.; Song, S.; Qiu, J.; Yi, L.; Cao, Z.; Li, J.; Cheng, S.; Wang, J., Viral Nonstructural Protein 1 Induces Mitochondrion-Mediated Apoptosis in Mink Enteritis Virus Infection. J Virol **93** (22) (2019).